# Declaration

I, **Honey Brahma**, hereby declare that the present thesis, entitled **Development of spectrum-based opto-electric-thermal model for reliable estimation of the energy yield of a photovoltaic module**, is the record of work done by me under the supervision of **Dr. Nabin Sarmah**, **Assistant Professor, Department of Energy, Tezpur University, Tezpur**. The contents of the thesis represent my original works that have not been previously submitted for any Degree/Diploma/Certificate in any other University or Institutions of Higher Education. This thesis is being submitted to Tezpur University for the Degree of Doctor of Philosophy in Energy.

Place: Tezpur University, Tezpur
Date: 07-06-2024

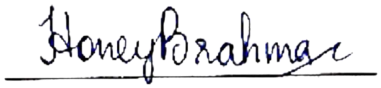

(Honey Brahma)

# TEZPUR UNIVERSITY

*(A Central University Established by an Act of Parliament)*
**Napaam, Tezpur-784028, Sonitpur, Assam, India**


# Certificate

This is to certify that the thesis entitled, ***Development of spectrum-based opto-electric-thermal model for reliable estimation of the energy yield of a photovoltaic module***, submitted to the School of Engineering, Tezpur University in partial fulfillment for the award of the degree of Doctor of Philosophy in Energy is a record of research work carried out by Ms. Honey Brahma under my supervision and guidance.

All help received by her from various sources has been duly acknowledged.

No part of this thesis has been submitted elsewhere for the award of any other degree.

07/06/2024

*(Supervisor)*

Dr. Nabin Sarmah
Assistant Professor, Department of Energy
School of Engineering, Tezpur University

March, 2024

# TEZPUR UNIVERSITY

*(A Central University Established by an Act of Parliament)*
**Napaam, Tezpur-784028, Sonitpur, Assam, India**

## Certificate of the External Examiner

This is to certify that the thesis entitled **"*Development of spectrum-based opto-electric-thermal model for reliable estimation of the energy yield of a photovoltaic module*"** submitted by **Ms. Honey Brahma,** Department of Energy, School of Engineering, Tezpur University in partial fulfillment for the award of the degree of Doctor of Philosophy in Energy has been examined by us on 07-06-2024 and found to be satisfactory.

The committee recommends the award of the degree of Doctor of Philosophy.

Supervisor
07/06/2024

(Dr. Nabin Sarmah)

Date: 07-06-2024

External Examiner

(Dr. N. SENDHILKUMAR)

Date: 07-06-24

# *Acknowledgements*

*I would like to express my gratitude to my PhD supervisor Dr. Nabin Sarmah for his guidance, support and ideas in completion of this thesis. I sincerely thank Dr. Greg P. Smestad, Principal at Sol Ideas Technology Development and Dr. Leonardo Micheli, Department of Astronautical, Electrical and Energy Engineering, Sapienza University of Rome for their encouragement, guidance and time to complete this reasearch work.*

*I am grateful to the members of the doctoral committee of my research Prof. D. Deka, Prof. S. Mahapatra, and Dr. N. Gogoi for their valuable comments and feedbacks during the progress seminars.*

*I acknowledge Tezpur University, Ministry of Tribal Affairs and India-UK Center for Education and Research in Clean Energy Project for the financial assistance that has made it possible for me to carry out my reasearch work.*

*I extend my thanks to the faculty members Prof. D. C. Baruah, Prof. R. Kataki, Dr. P.K. Choudhury, Dr. B. K. Kakati, and Dr. V. Verma and the technical staff Mr. M. Borah, Mr. T. Borah and Mr. T. Lahon of the Department of Energy, Tezpur University for their cordial, approcable nature, and help in laboratory work. I would also like to thank the office staff Ms. P. Rajbonshi and Mr. D. Bhuyan.*

*I would also like to extend my gratitude to Dr. P.K. Gogoi, Department of Applied Sciences for his suggestions in manuscript preparatio and Mr. P. Mudoi, Department of MBBT, Tezpur University, for his help in providing facilities to carry out some of my research work in CIF laboratory. Also, I am thankful to Assistant Librarian, Mr. Jitu Mani Das for his contribution in collection research materials and checking the similarity index.*

*I would like to thank my fellow research scholars of the Solar Energy Laboratory Barnam Jyoti Saharia, Pankaj Borah, and Hirock Jyoti Das and former M.Tech students Palash, Avik, Rabina, Arunava, Anjan, Puja, Debasish, Jyotish, Labanya, Shraiya for their help, support, encouragement, and creating healthy work place*

*I am also thankful to research scholars Jitu, Rishang, Rahul, Achyutish for their help and support.*

*I feel fortunate and would like to express my gratitude to my dear friends and sisters Minakshi, Panchali, Trinakshee, Adity, Saswati, Rangila, Mandira, Gayatri Ba, Sunny for sharing memorable time with me in the journey as a research scholar. Their presence have supported, motivated, and encouraged me both in academics and life.*

*A very special gratitude to my family members Maa, Baba, Maharaj (Babu), and Rewrewa for their constant support, inspiration, patience and understanding that have greatly aided me in reaching this point. Also, I would like to thank Almighty God for showering blessings upon me.*

***Honey Brahma***

*Dedicated*

*to*

*My Parents*

# List of figures


| | | Page No. |
|---|---|---|
| Figure 1.1 | Renewable accounts for total power capacity addition in the stated policies scenario (STEPS) over the 2022-2050 outlook period. (C&S: Central and South, APS: Announced Pledges Scenario). | 2 |
| Figure 1.2 | Typical absorption and scattering of incident sunlight at air mass one (AM1) under clear sky conditions. | 3 |
| Figure 1.3 | Solar spectrum for a range of wavelengths on the top of the atmosphere and the ground. | 4 |
| Figure 1.4 | Circuit diagram of solar cell highlighting the components. | 5 |
| Figure 1.5 | Different type of photovoltaic technologies. | 6 |
| Figure 1.6 | Efficiency of different types of solar cells over the last 35 years. | 6 |
| Figure 1.7 | Current-voltage (I-V) and power-voltage (P-V) curves of a PV module. | 9 |
| Figure 1.8 | Solar spectrum and external quantum efficiency (EQE) of the PV module. | 10 |
| Figure 1.9 | Various factors affecting solar photovoltaic performance. | 11 |
| Figure 1.10 | Layout of floating photovoltaic system along with their components. | 16 |
| Figure 2.1 | Distribution of solar spectrum used for electricity and heat generation in silicon solar cell. | 23 |
| Figure 2.2 | The electrical circuit of solar cell with (a) double-diode and (b) single-diode models | 25 |
| Figure 2.3 | Heat exchanges and physical phenomena in a photovoltaic module. | 29 |
| Figure 2.4 | Variation in transmittance and reflectance of incident light on the front glass of PV due to soiling (courtesy: Al Hicks/NREL). | 36 |
| Figure 2.5 | Trend on the number of studies related to different electrical, thermal, or optical modeling of PV. | 42 |
| Figure 3.1 | The overall flow of the work with three models, namely spectral, electrical, and thermal models along with the effect of soiling. | 43 |
| Figure 3.2 | Flowchart of model development. Here $T_{amb}$: air temperature, RH: relative humidity, t: time, $W_s$: wind speed, $\tau$: transmittance, EQE: external quantum efficiency, and $T_c$: cell temperature. | 44 |
| Figure 3.3 | Snapshot of the SMARTSv2.9.5 with the input configurations | 46 |

to generate the solar spectral irradiance of a site.

Figure 3.4 The step-by-step process in SMARTSv2.9.5. 46
Figure 3.5 The external quantum efficiency (EQE) of the monocrystalline and polycrystalline solar cells. Subscripts 'm' and 'p' denote the monocrystalline and polycrystalline, respectively. 49
Figure 3.6 Steps followed in COMSOL Multiphysics. 50
Figure 3.7 Different layers with various modes of heat transfer (left) and thermal network (right) of PV module. x is the thickness, k is the conduction heat transfer coefficient, and h represents the heat transfer coefficient. Subscripts f, c, b, amb, conv, rad, ext, and EVA denotes front, cell, back, ambient, convection, radiation, external, and ethylene-vinyl acetate, respectively. 51
Figure 3.8 (a) Geometry of the modeled m-Si PV module, (b) photograph of the m-Si PV module, (c) geometry of the modeled p-Si PV module, and (d) photograph of the p-Si PV module. 52
Figure 3.9 Mesh structure of PV module. 54
Figure 3.10 PV circuit diagram consisting of one-diode, series, and shunt resistance with solar spectrum and temperature as input parameters. 55
Figure 3.11 Flowchart of the novel methodology that can: (i) evaluate the variability of soiling and its seasonal correlations with environmental factors using the linear regression models, (ii) assess the effectiveness of the different cleaning cycles using the statistical t-test analysis, and (iii) evaluate the electrical characteristics of the PV module under soiling. 59
Figure 3.12 The Koppen-Geiger climate classification. 60
Figure 3.13 The average weekly value of the environmental parameters (a) particulate matter, PM10 ($\mu g/m^3$), (b) wind speed, $W_s$ (m/s), (c) dew point temperature, $T_d$ (°C), (d) ambient air temperature, $T_{amb}$ (°C), (e) relative humidity, RH (%), and (f) rainfall intensity, Rain (mm/day), which is equal to the direct average, over a given week, of the rainfall recorded in mm per minute multiplied by 60 minutes × 24 hours; (g) weekly frequency of rainfall $R_f$ (days). 62
Figure 3.14 Rose diagram for the wind direction of (a) pre-monsoon, (b) SW monsoon, (c) post-monsoon, and (d) winter seasons at the test site in Tezpur, India. 64
Figure 3.15 Photographs of the glass coupons placed outdoors having different cleaning cycles, weekly cleaned (G2), monthly cleaned (G3), and never cleaned (G4) (above), and an example of the non-uniform distribution of soiling observed, for 65

example, at week 45 (below).
Figure 3.16 Photograph of the UV-Vis spectrophotometer used in transmittance measurement of the glass coupons. 66
Figure 3.17 The photograph of the horizontally placed PV modules under the soiling. 70
Figure 3.18 Direct spectral irradiance and spectral response of the p-Si considered in the evaluation of the electrical performance of the soiled PV module under standard test conditions. 72
Figure 3.19 Schematic of the experimental setup showing the interconnection between different instruments. 77
Figure 3.20 Outdoor experimental setup at the Roof of the Department of Energy, Tezpur University, Tezpur, India for validation of the developed integrated spectrum-based model. 77
Figure 4.1 Generated solar spectrum using SMARTS at (a) various time of the day and (b) 12:00 local time during various seasons of the year. 82
Figure 4.2 Modeled (a) current-voltage and (b) power-voltage curves of the PV model under the varying solar spectrum. 83
Figure 4.3 Diurnal variations of (a) short-circuit current, $I_{sc}$ with spectral irradiance, and (b) open-circuit voltage, $V_{oc}$ with cell temperature of the PV module. Subscripts ‘m’ depicts m-Si, ‘p’ for p-Si, and ‘sim’ for simulation. 83
Figure 4.4 Variation in the *I-V* and *P-V* curve of the PV module due to varying cell temperature at constant irradiance of 595 W/m$^2$. 84
Figure 4.5 Temperature distributions (a) at an instant and (b) diurnal change in temperature at different layers (back surface, cell, and front glass surface) of the modeled PV module during the winter season 86
Figure 4.6 Temperature distributions (a) at an instant and (b) diurnal change in temperature at different layers (back surface, cell, and front glass surface) of the modeled PV module during the pre-monsoon season. 86
Figure 4.7 Representative relative solar-weighted transmittance of glass coupons with different cleaning schedules due to soiling during various seasons (a) winter, (b) post-monsoon, (c) south-west (SW) monsoon, and (d) pre-monsoon. 87
Figure 4.8 The average relative direct transmittance of glass coupons with different cleaning cycles (G2, G3, and G4) and total rainfall intensity in consecutive weeks of the year. 89
Figure 4.9 Frequency distribution of the average relative direct transmittance of the weekly cleaned, monthly cleaned and never cleaned glass coupons over the year. 90
Figure 4.10 Examples of the direct relative transmittance data fit to the 91-92

modified Ångström turbidity equation for glass coupons that exhibit (a) high $R^2$, (b) low $R^2$ values, and (c) direct transmittance of clean glass coupon with air as a reference. The data points are shown for the week and the spot on the coupon as indicated.

Figure 4.11 The average relative direct transmittance ($\tau_r$) versus offset parameter, c, of the modified Ångström turbidity equation for (a) selected weeks of the whole year and (b) the winter season. 93

Figure 4.12 The t-test p-value of a combination of seasons for the weekly cleaned (G2), monthly cleaned (G3), and never cleaned (G4) glass coupons. 95

Figure 4.13 The t-test analysis between different cleaning cycles: weekly cleaned, monthly cleaned, and never cleaned glass coupons for the monsoon (left) and non-monsoon (right) seasons. 96

Figure 4.14 The t-test analysis between different cleaning cycles: weekly cleaned, monthly cleaned, and never cleaned glass coupons for the low-soiling (left) and high-soiling (right) seasons. 96

Figure 4.15 Seasonal average transmittance loss ($\tau_{loss}$) and the respective standard deviation (in %) of weekly cleaned (G2), monthly cleaned (G3), and never cleaned (G4) glass coupons during the four seasons. 97

Figure 4.16 The average relative direct transmittance versus the weekly maximum rainfall ($R_{max}$) for the (a) G2 ($R^2 = 0.42$), (b) G3 ($R^2 = 0.40$), (c) G4 ($R^2 = 0.39$) and (d) the threshold rainfall required to clean the glass coupon under various cleaning schedule. 99

Figure 4.17 Correlation between the average relative direct transmittance ($\tau_r$), the average weekly *PM10*, and *RH* for the glass coupon with different cleaning cycles: (a) G2, (b) G3, and (c) G4. The figure on the right shows the scatter plot for data on the left. 100-101

Figure 4.18 Relation between average weekly relative direct transmittance ($\tau_r$), average weekly PM10 concentration, and (a) average weekly $\Delta T$, and (b) the number of hours in a week with the condition $T_d \geq (T_{amb} - 2.5\ °C)$ for the weekly cleaned glass coupon G2. 103

Figure 4.19 Regression plots of predicted transmittance and measured transmittance of weekly cleaned glass (G2) using an MLR model during the pre-monsoon season for various environmental parameters (a) $R_f$ and Ws, and (b) Rain and PM10. The uncertainty associated with the average relative direct transmittance of the weekly cleaned glass coupon during pre-monsoon is ±0.018. 105

Figure 4.20 Regression plot of predicted transmittance and measured 106

transmittance of weekly cleaned glass (G2) using a MLR model during post-monsoon season for the environmental parameters: (a) $R_f$, and (b) $W_s$. The uncertainty association with the average relative direct transmittance of the weekly cleaned glass coupon during post-monsoon is ±0.022.

Figure 4.21 Regression plot of predicted transmittance and measured transmittance of weekly cleaned glass (G2) using an MLR model during the winter season for various environmental parameters: (a) Rain and $W_s$, and (b) $R_{max}$ and $W_s$. The uncertainty associated with the average relative direct transmittance of the weekly cleaned glass coupon during winter is ±0.031. 107

Figure 4.22 Regression plot of predicted transmittance and measured transmittance of weekly cleaned glass (G2) using an MLR model for a year. The uncertainty associated with the average relative direct transmittance of the weekly cleaned glass coupon is ±0.02. The solid line represents the linear fit, and the dashed line represents an exponential fit with an offset to guide the eye (For the values of parameters of the linear and exponential fits, refer to tables 4.8 and 4.9, respectively.). 107

Figure 4.23 Relative transmittance of the glass coupons placed at horizontal (0°), vertical (90°), and tilted (26°) angles under the never cleaned condition. 109

Figure 4.24 Relative transmittance and normalized efficiency of the PV modules placed at (a) horizontal (0°) and (b) tilted (26°) angles. 110

Figure 4.25 I-V curve of the soiled PV module (at horizontal position) for various weeks. 111

Figure 4.26 Energy yield loss percentage due to soiling for different cleaning cycles during the four seasons and annually at STC. The "+" symbol denotes the (predicted) energy yield loss in $Wh/m^2/day$ for the right side y-axis. 111

Figure 4.27 Comparison of the simulated spectral irradiance generated using SMARTS and the measured spectral irradiance using spectrometer and pyranometer. 112

Figure 4.28 The linear fit between the predicted and measured global tilted irradiance (GTI) for (a) winter, (b) pre-monsoon, (c) SW monsoon, and (d) post-monsoon seasons. The $R^2$ of the predicted and measured spectral irradiance values for various seasons are presented in table 4.11. 113

Figure 4.29 The variation in measured cell temperature ($T_{c_m_exp}$) of PV module with global tilted irradiance (GTI), wind speed ($W_s$), and ambient temperature ($T_{amb}$) during (a) winter, (b) pre- 115

monsoon, (c) SW monsoon, and (d) post-monsoon.
Figure 4.30 Validation of the simulated back temperature of PV modules with the experimental back surface temperature for various seasons: (a) winter, (b) pre-monsoon, (c) SW monsoon, and (d) post-monsoon (subscript 'b' for back, 'm' for m-Si, 'p' for p-Si, 'sim' for simulation and 'exp' for experimental). 117
Figure 4.31 Validation of the simulated cell temperature of PV modules with the experimental cell temperature for various seasons: (a) winter, (b) pre-monsoon, (c) SW monsoon, and (d) post-monsoon (subscript 'c' for cell, 'm' for m-Si, 'p' for p-Si, 'sim' for simulation and 'exp' for experimental). 118
Figure 4.32 Validation of the I-V and P-V curves of a m-Si PV module. 119
Figure 4.33 The experimental and simulated $I_{sc}$ and $V_{oc}$ values of m-Si for (a) winter, (b) pre-monsoon, (c) SW monsoon, and (d) post-monsoon days. 120
Figure 4.34 The linear fit between the short-circuit current ($I_{sc}$) and global irradiance (G) during various seasons for m-Si and p-Si. 121-122
Figure 4.35 (a) Comparison of simulated and experimental $P_{max}$ and (b) linear fit between the maximum power and global irradiance, during winter season. RE is the relative error. 123
Figure 4.36 (a) Comparison of simulated and experimental $P_{max}$ and (b) linear fit between the maximum power and global irradiance, during pre-monsoon season. RE is the relative error. 123
Figure 4.37 (a) Comparison of simulated and experimental $P_{max}$ and (b) linear fit between the maximum power and global irradiance, during SW monsoon season. RE is the relative error. 123
Figure 4.38 (a) Comparison of simulated and experimental $P_{max}$ and linear fit between the maximum power and global irradiance (right), for post-monsoon season. RE is the relative error. 124
Figure 4.39 Validation of the energy yield obtained from the m-Si and p-Si PV modules for various seasons. 126
Figure 4.40 Typical **e**nergy yield of m-Si PV module under clean and soiled conditions for cleaning cycles (weekly: G2, monthly: G3, and never cleaned: G4, as described in section 4.2). 126
Figure 4.41 Energy yield of p-Si PV module under clean and soiled conditions for cleaning cycles (weekly: G2, monthly: G3, and never cleaned: G4, as described in section 4.2). 127

# List of tables


| | | Page No. |
|---|---|---|
| Table 3.1 | The seasonal value of the environmental parameters input to SMARTSv2.9.5 during various seasons. | 47 |
| Table 3.2 | Thermophysical properties and dimensions of the materials. | 50 |
| Table 3.3 | Distribution (percentage of total days) of wind speed for each of the four seasons. | 64 |
| Table 3.4 | Specifications of the p-Si PV module used in the experiment setup to investigate the soiling effect. | 70 |
| Table 3.5 | Specification of the p-Si and m-Si PV modules used in the experimental validation. | 76 |
| Table 3.6 | Specification of the instruments used in the experimental validation of the developed models. | 78 |
| Table 4.1 | Variation of open-circuit voltage, short-circuit current and power output with cell temperature at constant irradiance of 595 $W/m^2$. | 85 |
| Table 4.2 | The seasonal and annual average transmittance loss ($\tau_{loss}$ in %), the average seasonal uncertainty (u in %), and seasonal average standard deviation (SD in %) in the average relative direct transmittance ($\tau_r$) of different glass coupons. | 91 |
| Table 4.3 | The F-test and t-test (two sample results assuming unequal variance) statistical analysis for different combination of glass coupons. The results compare the weekly cleaned (G2), monthly cleaned (G3), and never cleaned (G4) glass coupons. | 94 |
| Table 4.4 | The value of the indicated parameters and the $R^2$ value obtained from the logistic curve fitting for the average relative direct transmittance of the glass coupons vs. the weekly maximum rainfall $R_{max}$, for different cleaning cycles: G2, G3 and G4. | 100 |
| Table 4.5 | The value of the indicated parameters and the $R^2$ value obtained from the linear curve fitting for the average relative direct transmittance ($\tau_r$) vs. average air temperature ($T_{amb}$) for the weekly cleaned (G2), monthly cleaned (G3), and never cleaned (G4) glass coupons for the whole year. | 102 |
| Table 4.6 | The value of the indicated parameters and the $R^2$ value obtained from the linear curve fitting for the average relative direct transmittance ($\tau_r$) vs. the average dew point temperature ($T_d$) for G2, G3, and G4 glass coupons for the whole year. | 103 |

| | | |
|---|---|---|
| Table 4.7 | The correlation values obtained using single-variable linear regression (SLR) models between the average relative direct transmittance of the weekly cleaned glass coupon (G2) and the average weekly value of various environmental parameters: rainfall intensity (Rain), frequency of rainfall ($R_f$), relative humidity (RH), particulate matter (PM10), ambient air temperature ($T_{amb}$) and dew point temperature ($T_d$). The analysis is performed using the data for a full year. | 104 |
| Table 4.8 | Values for the linear fit parameters for the annual analysis using MLR. This is used for the regression plot of predicted and measured transmittance for the weekly cleaned glass (G2) using an MLR model for the whole year. | 107 |
| Table 4.9 | Values for the exponential fit parameters for the annual analysis using MLR. This is used for the regression plot of predicted and measured transmittance for the weekly cleaned glass (G2) using an MLR model for the whole year. | 107 |
| Table 4.10 | The seasonal analysis result of the MLR model in correlating the average relative direct transmittance of the weekly cleaned glass (G2) and the environmental parameters with p-value < 0.05. | 109 |
| Table 4.11 | Average value of the simulated and measured global tilted irradiance and coefficient of determination ($R^2$) value | 114 |
| Table 4.12 | Average value of $W_s$, $T_{amb}$, and $T_c$ (for m-Si and p-Si PV modules) for during various seasons. | 115 |
| Table 4.13 | Statistical errors of the developed thermal model in terms of $T_b$ value for various seasons. | 117 |
| Table 4.14 | Statistical errors of the developed thermal model in terms of $T_c$ value for various seasons. | 119 |
| Table 4.15 | Statistical errors of the $I_{sc}$ and $V_{oc}$ values of the m-Si PV module. | 121 |
| Table 4.16 | Statistical errors of the $I_{sc}$ and $V_{oc}$ values of the p-Si PV module. | 121 |
| Table 4.17 | Statistical errors namely MAE, MRE, RMSE and $R^2$ of the $P_{max}$ of p-Si and m-Si PV modules during various seasons. | 124 |
| Table 4.18 | Comparative analysis of statistical error (RMSE) of PV module parameters with previously reported models. | 125 |
| Table 4.19 | The percentage change in simulated energy yield in comparison to experimental energy yield for m-Si and p-Si under varying seasons. | 126 |
| Table 4.20 | Percentage deviation in the energy yield of the m-Si and p-Si under soiled conditions (different cleaned cycles) compared to clean conditions for various seasons. | 127 |

# List of abbreviations

| Abbreviation | Description |
|---|---|
| AM | air mass |
| AOD | aerosol optical depth |
| APS | Announced Pledges Scenario |
| ARC | anti-reflective coating |
| ASPIRE | All-sky Spectral IRadiancE |
| BC-BJ | Back Contact-Back Junction |
| BDF | Backward Differentiation Formula |
| CdTe | cadmium telluride |
| CIS | copper indium diselenide |
| CIGS | copper indium gallium selenide |
| CZ | Czochralski |
| C&S | Central and South |
| DSSC | dye-sensitized solar cells |
| EoT | equation of time |
| EQE | external quantum efficiency |
| EVA | ethylene-vinyl acetate |
| FF | fill factor |
| GDP | gross domestic product |
| GTI | global tilted irradiance |
| HIT | Heterojunction with Intrinsic Thin layer |
| IEA | International energy agency |
| I-V | current-voltage |
| LID | light-induced degradation |
| LST | local solar time |
| LSTM | local standard time meridian |
| LT | local time |
| MAE | mean absolute error |

| | |
|---|---|
| MAPE | mean absolute percentage error |
| MLR | multi-variable linear regression |
| MPP | maximum power point |
| MRE | mean relative error |
| MSE | mean square error |
| NOCT | nominal operating cell temperature |
| OPV | organic photovoltaic |
| PV | photovoltaic |
| P-V | Power-voltage |
| QDSC | quantum dot solar cells |
| RMSE | root mean square error |
| SBDART | Santa Barbara DISORT Atmospheric Radiative Transfer |
| SD | standard deviation |
| SLR | single-variable linear regression |
| SMARTS | Simple Model of the Atmospheric Radiative Transfer of Sunshine |
| SPCTRAL2 | Simple Solar Spectral Model for Direct and Diffuse Irradiance on Horizontal and Tilted Planes at the Earth's Surface for Cloudless Atmospheres |
| SR | spectral response |
| STC | standard test conditions |
| STEPS | stated policies scenario |
| SW | South-west |
| TC | time correction factor |
| TRNSYS | transient system simulation |
| u | uncertainty |
| UTC | universal coordinated time |
| UV | ultraviolet |

# List of symbols and subscripts

## Symbols

| Notation | Description |
|---|---|
| A | active area |
| a-Si | amorphous silicon |
| $\alpha$ | elevation angle |
| B | breadth |
| $\beta$ | slope |
| c | speed of light |
| $c_p$ | heat capacity at constant pressure |
| d | $i^{th}$ day of the year |
| D | diffusivity of minority carrier |
| $\delta$ | declination angle |
| E | energy yield |
| $E_G$ | bandgap |
| $\varepsilon$ | emissivity |
| G | incident global spectral irradiance |
| $G_o$ | total absorbed solar spectrum |
| $G_r$ | reference solar irradiance |
| $G_T$ | total irradiance |
| $\gamma$ | surface azimuth angle |
| h | Planck's constant |
| $h_{conv}$ | convective heat transfer coefficient |
| $h_{rad}$ | radiative heat transfer coefficient |
| $H_s$ | sunshine hour |
| I | current |
| $I_{mp}$ | maximum current |
| $I_o$ | diode saturation current |
| $I_{ph}$ | photocurrent |

| | |
|---|---|
| $I_{sc}$ | short circuit current |
| $J_{sc}$ | short-circuit current density |
| k | conductive heat transfer coefficient |
| $k_B$ | Boltzmann's constant |
| K | extinction coefficient |
| $K_i$ | temperature coefficient for short-circuit current |
| $K_v$ | temperature coefficient for open-circuit voltage |
| L | length |
| $L_d$ | minority carrier diffusion length |
| $L_p$ | path length |
| η | efficiency |
| $\eta_{normlized}$ | normalized efficiency |
| $\eta_{PV(EQE,T)}$ | efficiency of the PV module |
| $\eta_{PV(EQE,T)t=0}$ | efficiency at the initial conditions |
| n | ideality factor |
| $n_i$ | intrinsic carrier concentration |
| $n_1$ | refractive indices of air |
| $n_2$ | refractive indices of glass |
| $N_D$ | doping concentration |
| $N_s$ | number of cells connected in series |
| m | air mass |
| m-Si | monocrystalline silicon |
| λ | wavelength |
| P | power |
| $P_{incident}$ | incident power |
| $P_{max}$ | maximum power |
| PM | particulate matter |
| p-Si | polycrystalline silicon |
| ρ | density |
| q | electronic charge |
| $q_c$ | heat flux by conduction |
| $q_{cond}$ | conductive heat transfer |
| $q_{conv}$ | convective heat transfer |

| | |
|---|---|
| $q_r$ | heat flux by radiation |
| Q | additional heat source |
| $Q_{ted}$ | thermoelastic damping |
| $r_s$ | soiling ratio |
| Rain | rainfall |
| $R^2$ | coefficient of determination |
| $R_f$ | frequency of rainfall |
| RE | relative error |
| RH | relative humidity |
| $R_{max}$ | maximum rainfall |
| $R_s$ | series resistance |
| $R_{sh}$ | shunt resistance |
| $R_{shn}$ | intermediate values of shunt resistance |
| $R_{sho}$ | initial shunt resistances |
| $R_{sn}$ | intermediate values of series resistance |
| $R_{so}$ | initial series resistances |
| Si | silicon |
| SW | South-west |
| t | time |
| T | temperature |
| $T_{amb}$ | ambient temperature |
| $T_c$ | cell temperature |
| $T_d$ | dew point temperature |
| $T_{ext}$ | external temperature |
| $T_r$ | reference temperature |
| $\tau$ | transmittance |
| $\tau_{absor}$ | transmittances due to the absorption of glazing |
| $\tau_{loss}$ | soiling transmittance loss |
| $\tau_r$ | relative direct transmittance |
| $\tau_{reflec}$ | transmittances due to the reflection of radiation |
| $u_{trans}$ | translational motion velocity vector |
| V | voltage |
| $V_{mp}$ | maximum voltage |

| | |
|---|---|
| $V_{oc}$ | open-circuit voltage |
| $V_{th}$ | thermal voltage |
| $W_s$ | wind speed |
| $\omega$ | hour angle |
| x | thickness |
| $\theta$ | zenith angle |
| $\theta_1$ | angles of incidence |
| $\theta_2$ | angles of refraction |
| $\varphi$ | latitude |
| $\sigma$ | Stefan Boltzmann constant |

## Subscripts

| **Notation** | **Description** |
|---|---|
| amb | ambient |
| b | back |
| c | cell |
| clean | under clean condition |
| conv | convection |
| exp | experiment |
| ext | external |
| f | front |
| m | monocrystalline |
| max | maximum |
| p | polycrystalline |
| rad | radiative |
| $r_s$ | soiling ratio |
| sim | simulation |
| soiled | under soiled condition |